Bioelectrochemistry 82 (2011) 87–94

Contents lists available at ScienceDirect

Bioelectrochemistry

journal homepage: www.elsevier.com/locate/bioelechem

A novel H_2O_2 amperometric biosensor based on gold nanoparticles/self-doped polyaniline nanofibers

Xiaojun Chen [a], Zixuan Chen [a], Jinwei Zhu [a], Chenbin Xu [a], Wei Yan [b], Cheng Yao [a,*]

[a] College of Sciences, Nanjing University of Technology, Nanjing, 210009, PR China
[b] Nano Science and Technology Research Center, Shanghai University, Shanghai, 200444, PR China

ARTICLE INFO

Article history:
Received 19 January 2011
Received in revised form 7 May 2011
Accepted 23 May 2011
Available online 1 June 2011

Keywords:
Gold nanoparticles/self-doped polyaniline nanofibers
Horseradish peroxidase
H_2O_2
Biosensor

ABSTRACT

A new kind of gold nanoparticles/self-doped polyaniline nanofibers (Au/SPAN) with grooves has been prepared for the immobilization of horseradish peroxidase (HRP) on the surface of glassy carbon electrode (GCE). The ratio of gold in the composite nanofibers was up to 64%, which could promote the conductivity and biocompatibility of SPAN and increase the immobilized amount of HRP molecules greatly. The electrode exhibits enhanced electrocatalytic activity in the reduction of H_2O_2 in the presence of the mediator hydroquinone (HQ). The effects of concentration of HQ, solution pH and the working potential on the current response of the modified electrode toward H_2O_2 were optimized to obtain the maximal sensitivity. The proposed biosensor exhibited a good linear response in the range from 10 to 2000 μM with a detection limit of 1.6 μM (S/N = 3) under the optimum conditions. The response showed Michaelis–Menten behavior at larger H_2O_2 concentrations, and the apparent Michaelis–Menten constant K_m was estimated to be 2.21 mM. The detection of H_2O_2 concentration in real sample showed acceptable accuracy with the traditional potassium permanganate titration.

1. Introduction

Advances in nanofibers offer new directions in the design and development of electronic devices including field-effect transistors, sensors, catalyst supports, solar cells, light-emitting diodes, and so on [1–5]. Owing to their dimensions in the range of 100 nm and high surface-to-volume ratios, nanofibers display unique physical and chemical properties. Considerable attention has been paid to the application of nanofibers in the bioanalysis and biosensors [6]. Recently, Ahmad et al. fabricated a highly sensitive glucose biosensor based on a single ZnO nanofiber and obtained detection limit low to 1 μM [7]. Zhang and his coworkers prepared a novel gold nanoparticle-bacteria cellulose nanofiber via a one-step method, and a novel H_2O_2 biosensor was constructed using the obtained nanofiber, which allows the detection of H_2O_2 with a detection limit lower than 1 μM [8]. Sheng et al. combined porous carbon nanofiber and room-temperature ionic liquid to provide a suitable microenvironment for immobilizing heme-proteins, and the modified electrode could catalyze the reduction of O_2, H_2O_2 and nitrite [9].

Electrochemical biosensors have been developed to be the most promising detection scheme owing to the advantages of simplicity, high reliability, sensitivity and selectivity, low cost, fast response, and ease of use [10,11]. Nanofibers with unique merits such as aspect ratio, size scale and tunable electron transport, are widely used as ideal substrate to improve the performance of electrochemical biosensors. To achieve high-performance electrochemical biosensors, it is desired that the nanofibers have the acceptable biocompatibility and good electrical properties. The modification of noble metal nanoparticles on the nanofiber surface or the coat of biomimetic silica is an effective approach to improve the performance of biosensors due to the highly catalytic activity of noble metal and the high biocompatibility of silica matrix to maintain the nature characteristics of enzymes [12–14].

Conducting polymers have been widely investigated due to their special electrical property for the applications in electrocatalysis, capacitors, sensors, fuel cells, and corrosion protection [15–18]. As one of the most important conducting polymers, polyaniline (PANI) has attracted significant interests in view of its considerable flexibilities in modifying its chemical structures, compatibility with biological molecules in neutral aqueous solutions, and the ability to efficiently transfer the electric charges produced by biochemical reactions to electronic circuits. These advantages are favorable to its application in rechargeable batteries [19,20], electrocatalysis [21–24] and biosensors [25,26]. However, the limitation that PANI shows electro-activity only in acidic medium restricts its potential applications, especially in bioelectrochemistry, which usually requires the near-neutral environment. To solve the problem, self-doped PANI (SPAN) was first synthesized by Yue and Epstein, which could maintain its electroactivity even up to basic medium [27]. Thereafter, various SPAN nano-

* Corresponding author. Tel./fax: +86 25 83587433.
E-mail address: xiaojunchen_njut@163.com (C. Yao).

1567-5394/$ – see front matter © 2011 Elsevier B.V. All rights reserved.
doi:10.1016/j.bioelechem.2011.05.004

materials have been explored and applied to construct biosensors. Zhang synthesized o-aminophenol or p-phenylenediamine doped PANI for the detection of ascorbic acid or H_2O_2[28,29]. Wang et al. reported a flower-like SPAN by electrochemical copolymerization of aniline and o-aminobenzenesulfonic acid, and investigated its improved electro-activity [30]. Zhang and coworkers designed a novel Fe_2O_3/SPAN nanofibers/carbon ionic liquid electrode for impedance sensing of DNA hybridization [31]. However, there are few reports on the gold/SPAN nanofibers for constructing a highly sensitive enzyme biosensor.

Hydroquinone (HQ) is an excellent electron mediator, which efficiently reduces the working potential and eliminates the effects of various electro-active substances in real samples; it has been successfully used in numerous peroxidase-based amperometric biosensors to detect H_2O_2[32,33]. In this paper, SPAN nanofibers with grooves were chemically synthesized by copolymerization of aniline and 3-aminobenzenesulfonic acid. Due to the effective doping of oxygen-containing functionalities, especially of sulfonic acid groups, on the surface of SPAN nanofibers, the electro-activity of PANI has been extended to neutral medium, and the unique structure of grooves increased the active surface area of conductive SPAN. Then, gold nanoparticles were modified on the surface of SPAN fibers through electrostatic adsorption and the ratio of gold in the Au/SPAN composites was up to 64%, which promoted its conductivity and biocompatibility greatly. As an example, horseradish peroxidase (HRP) was successfully immobilized on Au/SPAN nanofibers modified glassy carbon electrode (GCE). For the first time an amperometric H_2O_2 biosensor was fabricated on the basis of HRP-Au/SPAN compound modified electrode with HQ as mediator.

2. Experimental

2.1. Materials

Aniline (AN) was distilled twice under reduced pressure and stored in dark at low temperature before use. The supporting electrolyte phosphate buffer saline (PBS, 0.1 M) was prepared by mixing the stock solutions of KH_2PO_4 and K_2HPO_4, and adjusted to appropriate pH by the addition of 0.1 M NaOH or H_3PO_4 solution. 250 U mg^{-1} HRP (EC 1.11.17) was purchased from Sigma. Stock solution of 2 mg mL^{-1} HRP was prepared in pH 7.0 PBS and stored at 4 °C. Glutaraldehyde (GA, 25 wt.%) was supplied by Chengdu Kelong Chemical Reagents. Poly (diallyldimethylammonium chloride) (PDDA, 20 wt.%) and chitosan (CS) were purchased from Aldrich. Stock solution of 0.20 wt.% PDDA was prepared in deionized water with Tris and NaCl. CS solution was prepared by dissolving CS flakes in 1% acetic acid. H_2O_2 (30% w/v solution) was obtained from Sinopharm Chemical Reagent Co. Ltd., and its accurate concentration was determined by titration with potassium permanganate. 3-Aminobenzenesulfonic Acid (SAN) was purchased from TCI. Cetyl trimethyl ammonium bromide (CTAB), ammonium persulfate (APS), potassium ferricyanide ($K_3[Fe(CN)_6]$), potassium ferrocyanide ($K_4[Fe(CN)_6]$) and potassium chloride (KCl) were all purchased from Shanghai Linfeng Chemical Reagent Co. Ltd. The CV and EIS measurements were performed in the presence of 2 mM $[Fe(CN)_6]^{3-/4-}$ containing 0.1 M KCl. Chloroauric acid hydrated ($HAuCl_4$•$4H_2O$) was purchased from Nanjing Chemical Reagent Co. Ltd. Other reagents were of analytical grade and used without further purification. All the solutions were prepared with double distilled water.

2.2. Instruments

The size of SPAN and Au/SPAN was determined by transmission electron microscopy (TEM, JEOL JEM-200CX) and field-emission scanning electron microscopy (FESEM, HITACHI S4800). Fourier-transform infrared (FT-IR) spectroscopic measurements were performed on a Bruker model VECTOR22 Fourier-transform spectrometer using KBr pressed disks. Thermo-gravimetric analysis (TGA) was performed on NETZSCH STA 449C. Zeta potential analysis was performed with a PALS Zeta Potential Analyzer, version 3.43 (Brookhaven Instruments Corp.). The conductivities of the samples were measured by a four-probe method using a WR-2B digital multimeter at room temperature in air atmosphere. Nitrogen adsorption and desorption isotherms were measured at −196 °C with a Micromeritics ASAP 2020 analyzer. The specific surface area was determined using the standard Brunauer–Emmett–Teller (BET) method.

2.3. Construction of H_2O_2 biosensor

2.3.1. Preparation of Au/SPAN nanofiber

The preparation of SPAN nanofiber was similar to that in the previous report [34]. In brief, 0.11 g CTAB was dissolved in 40 mL of 0.15 M HCl with 0.23 g AN and 0.43 g SAN, followed by adding 20 mL of APS solution with a concentration of 0.06 M. The copolymerization reaction was carried out under static conditions at 4 °C for 24 h. The resulting dark green precipitates were centrifuged and washed 3 times with doubly distilled water and ethanol successively.

The Au colloid was prepared as described in literature [35]. In a typical synthesis, 5 mL of 1% $HAuCl_4$ and 10 mL of 0.03 M sodium citrate were mixed in 250 mL of doubly distilled water, followed by added 5 mL of freshly prepared 0.1 M KBH_4. After the solution color turned to wine red, stirring was stopped and the solution was left undisturbed for at least 2 h. The Au colloid was stored at 4 °C. The "negatively" charged SPAN fibers with a ζ-potential of −6.5 mV, indicating large amount of $–SO_3H$ groups doped on the surface of SPAN. Then, SPAN was dispersed in PDDA solution under stirring for 20 min to achieve positive charged modification. After washed with water, it was spread in 250 mL Au colloid solution and stirred for 8 h. After centrifugation, the dark red Au/SPAN nanocomposite was obtained after washed 3 times with doubly distilled water and dried in a vacuum oven at 40 °C for 24 h.

2.3.2. Fabrication of Au/SPAN-HRP-CS/GCE

Prior to the electrode modification, the GCE was polished with 1.0, 0.3, and 0.05 μm α-Al_2O_3 powder, and then rinsed thoroughly with ethanol and doubly distilled water until a mirror-like surface was obtained. 10 μL of Au/SPAN nanofibers (1 mg mL^{-1}, CS solution) was mixed with 10 μL of HRP stock solution and 5 μL of 2.5 wt.% GA water solution. Then, 10 μL of the mixture was cast onto the GCE. The resulting Au/SPAN-HRP-CS/GCE obtained after modification of the electrode was dried in air at 4 °C for 12 h and immersed in a pH 7.0 PBS for 30 min to remove the redundant adsorbed HRP before use.

2.4. Electrochemical measurements

Electrochemical experiments were performed at room temperature on a CHI 660D electrochemical workstation (Shanghai CH Instrument Co.) in a conventional three-electrode electrochemical cell using modified or bare GCE (Φ = 3.0 mm) as working electrode, a twisted platinum wire as auxiliary electrode, and a saturated calomel reference electrode (SCE) as reference electrode against which all potentials were measured in this paper. For steady-state amperometric experiments, the working potential was set at −0.15 V and the solution was stirred gently with a magnetic stirrer. Before each electrochemical measurement, the experimental solution in the cell was purged with highly purified nitrogen gas for at least 20 min to remove dissolved oxygen and then a nitrogen atmosphere was kept over the solution during measurements.

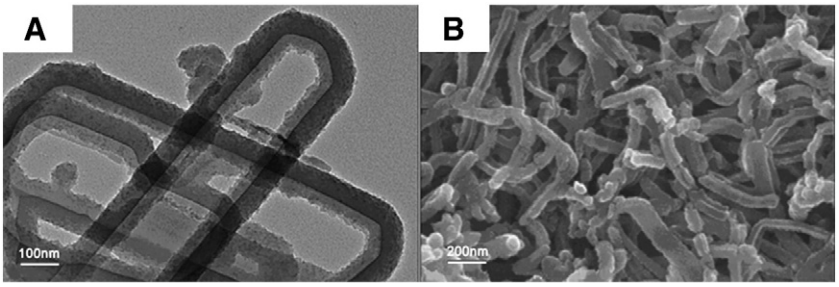

Fig. 1. TEM (A) and SEM (B) images of SPAN nanofibers.

3. Results and discussion

3.1. Characterization of Au/SPAN nanofibers

The morphological characters of prepared SPAN nanofibers were obtained by SEM and TEM, as shown in Fig. 1. SPAN nanofibers have a uniform size with a diameter of 60–70 nm while the length was up to several micrometers. Moreover, it could be observed from Fig. 1B, SPAN nanofibers have obvious grooves along the length axis, indicating that are formed by bending the SPAN nanobelts [34]. To understand the formation process of SPAN nanofibers synthesized by the "in situ doping polymerization," the TEM images of SPAN nanofibers synthesized at different reaction time were measured and shown in Fig. 2. In the first 1 h (Fig. 2A), the aniline gathered first to polymerize and form the flakes or slices with a width of around 100 nm. In the next 4 h for reaction, these polymer flakes incorporated and grew which resulted in the appearance of long nanobelts (Fig. 2B). As the polymerization had lasted for 8 h, these nanobelts above curled and the initial grooves were obtained (Fig. 2C). With the reaction sustained for 24 h, the final product was obtained as a kind of nanofiber with grooves along the length axis, which would make the nanofibers have a larger surface area and was determined to be 11.1 $m^2 g^{-1}$ (Fig. 2D). Fig. 3 shows the TEM and SEM morphologies of Au/SPAN nanofibers with a diameter increased to 90–100 nm, which was attributed to the compact wrap of Au nanoparticles on the surface of SPAN nanofibers. Moreover, when Au/SPAN was modified on the surface of GCE, most of fibers bended and formed loose and porous networks which would result in a stable structure for immobilizing HRP.

The nature of the Au/SPAN nanofibers was further proved by FT-IR spectrum. As shown in Fig. 4, all of the characteristic peaks of SPAN were displayed. In detail, the peaks at 1640 and 1458 cm^{-1} are characteristic of the C=C stretching vibration of quinoid and benzenoid rings, respectively. The C–N stretching of secondary aromatic amines (1274 cm^{-1}), and the aromatic C–H bending (1218 cm^{-1}) are also observed [36,37]. The bands at 1087, 686 and 614 cm^{-1} are attributed by the O=S=O, S–O and C–S stretching vibration, respectively. Moreover, the peak observed at 833 cm^{-1} reveal the presence of 1, 2, 4-trisubstitution of aromatic ring [38]. These peaks proved the existence of the $–SO_3H$ groups bonding to the phenyl rings.

TGA was used to determine the weight percentage of gold in the Au/SPAN, as shown in Fig. 5, curve b. For comparison, the TGA curve of original SPAN was also presented as curve a. The residual wt.% refers to the weight percentage content of Au in the composite. The TGA curve of SPAN shows a two-step weight loss. The weight loss in the first step is attributed to the loss of residual water. The second step that starts at around 300 °C corresponds to polymer degradation [39]. The total weight loss of SPAN is 100% under these experimental conditions. In the case of Au/SPAN nanofibers, TGA curve shows a three-step weight loss. The first weight loss is consistent with the SPAN. The second weight loss, which ranges from 200 to 300 °C, is believed to be caused by the departure of a part of SAN, and the third weight loss step is attributed to the decomposition of SPAN chains and the departure of residual SAN. The residual mass of the Au/SPAN composite was about 64%, which might be due to the strong electrostatic effect between PDDA functionalized SPAN and Au nanoparticles.

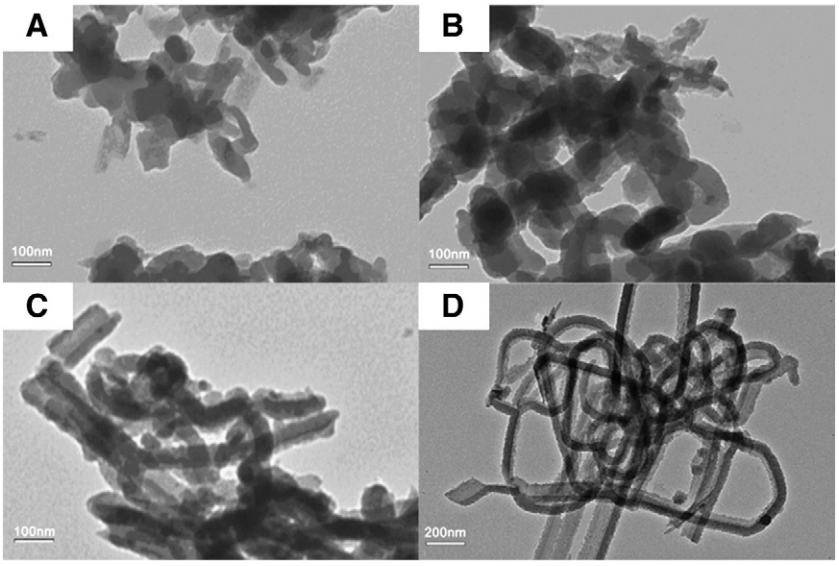

Fig. 2. TEM images of different polymerization stages of SPAN nanofibers: (A) 1 h, (B) 4 h, (C) 8 h and (D) 24 h.

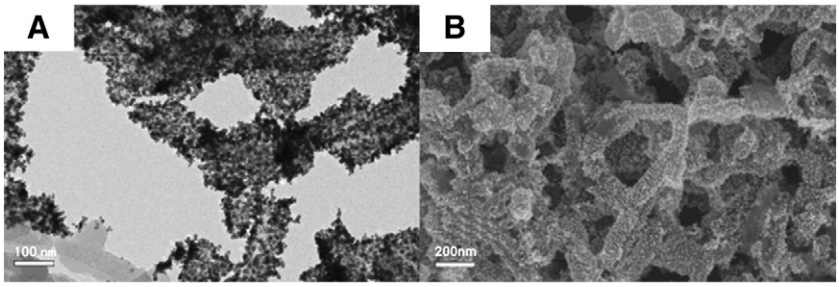

Fig. 3. TEM (A) and SEM (B) images of Au/SPAN nanofibers.

Also, the conductivity of the Au/SPAN was found to be 0.22 S/cm, whereas that of SPAN was found to be 3.4×10^{-4} S/cm. Thus, there was an increase of about three orders of magnitude in conductivity upon incorporation of gold in the conductive form of SPAN using the present method. Because gold is a conductor, it is beneficial for improving the conductivity of SPAN when it is doped with gold.

3.2. Redox electro-activity of SPAN-CS/GCE

For pure PANI, it is only electro-active when the pH is lower than 4.0, while the electro-activity of the copolymer SPAN is greatly improved. As shown in Fig. 6, the SPAN-CS/GCE shows redox peaks in solution with pH values from acid to weak base. From pH 5.0 to 9.0, the two sets of peaks overlap into one pair of peaks, which corresponds to the leucoemeraldine/pernigraniline reaction. When the medium pH increases up to 7.0, the redox electro-activity of PANI still remains, indicating the effective extension for the electrochemical activity of PANI. This improvement may be due to the doping of oxygen-containing functionalities on SAN into PANI backbone. The presence of $-SO_3H$ groups can change the microenvironment of SPAN, it can be assumed that when there is an increase in medium pH, the H^+ ion in $-SO_3H$ groups can take a role of "buffer" and maintain the local pH value to some extent in SPAN nanofibers near the electrode surface. Thus, the SPAN can still exhibit electrochemical activity in solution with higher pH value.

3.3. Electrochemical characterization of the electrode surface

All electrochemical measurements were performed in pH 7.0 PBS solution containing 0.1 M KCl and 2 mM $Fe(CN)_6^{3-}$/ $Fe(CN)_6^{4-}$. The CV of ferricyanide was chosen as a marker to investigate the changes of the electrode behavior after each modification step. Fig. 7A shows the CV of $Fe(CN)_6^{3-}$/$Fe(CN)_6^{4-}$ at the bare GCE (curve a), SPAN-CS/GCE (curve b), Au/SPAN-CS/GCE (curve c) and Au/SPAN-HRP-CS/GCE (curve d), respectively. Comparing the current response obtained at these modified electrodes, the results suggest that both SPAN and Au nanoparticles could promote the electrochemical response to some extent, which indicated that the SPAN and Au nanoparticles modified electrodes had much larger effective surface area and good electric conductivity. After the Au/SPAN-CS film was used to modify GCE, the largest peak current value and the smallest peak-to-peak separation (ΔE_p) were obtained, which also could be deduced that the synergistic effects of Au nanoparticles and SPAN might facilitate the electron transfer between electrode surface and electro-active probe molecules. The immobilization of HRP on the electrode surface was accompanied by a decrease in the amperometric response and an increase in ΔE_p, which was attributing to the insulating property of the protein layer.

Electrochemical impedance spectroscopy (EIS) can also provide detailed information about the impedance changes of the electrode surface during the fabrication process. The Nyquist plot of the EIS includes a semicircular portion and a linear portion. The semicircular portion at higher frequencies corresponds to the electron-transfer-limited process and its diameter is equal to the electron-transfer resistance (R_{et}), which controls the electron-transfer kinetics of the redox probe at the electrode interface. Meanwhile, the linear part at lower frequencies corresponds to the diffusion process. Changes of the impedance spectra were observed in the course of stepwise modification of the electrode, as shown in Fig. 7B, and the R_{et} values of the bare GCE (curve a) were estimated to be 411 Ω. When the SPAN-CS (curve b) and Au/SPAN-CS (curve c) were modified on the bare GCE, their R_{et} values declined to 158 and 88 Ω, respectively, which indicated that Au nanoparticles have good conductivity and that the Au/SPAN composite can make the electron transfer easier

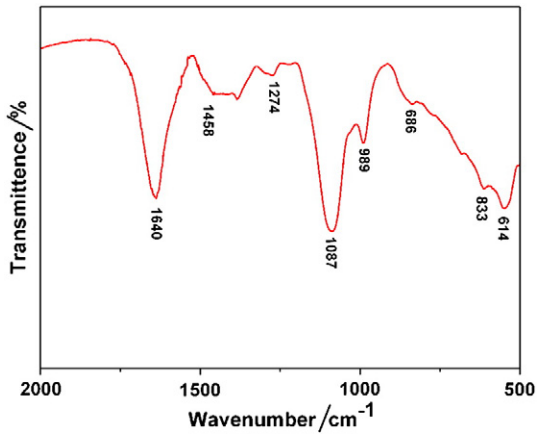

Fig. 4. FT-IR spectrum of Au/SPAN nanofibers.

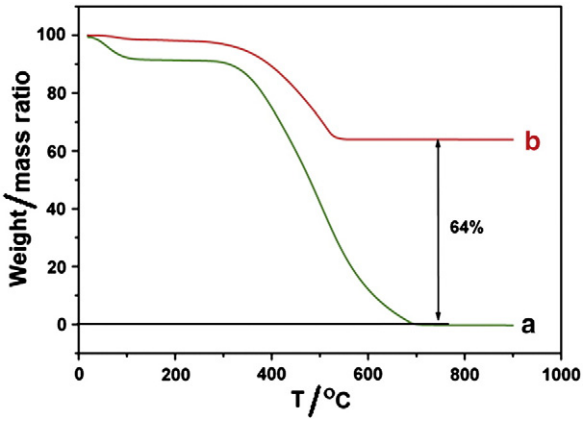

Fig. 5. TGA curves for (a) SPAN and (b) Au/SPAN nanofibers.

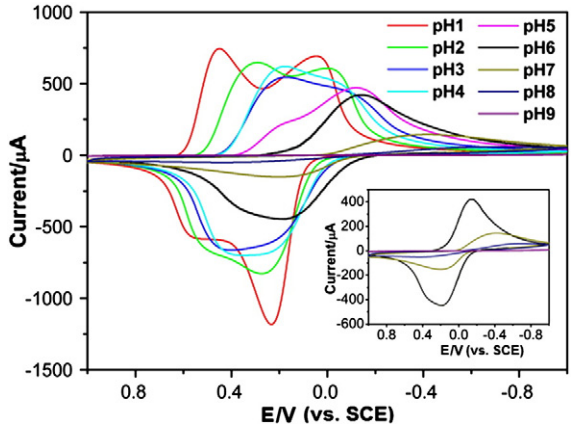

Fig. 6. CVs of SPAN-CS/GCE in solutions with different pH values at 100 mV/s.

while the R_{et} value of Au/SPAN-HRP-CS/GCE (curve d) was increased to 704 Ω.

3.4. Optimization of experimental parameters

In order to maximize the detection sensitivity of the proposed H_2O_2 biosensor, we optimized various conditions, including the concentration of the mediator, solution pH, the working potential of chornoamperometry and the temperature, via changing the examined condition while the others were fixed.

First, the biosensor response was studied in 0.1 M pH 7.0 PBS containing different concentrations of HQ using steady-state amperometry at −0.15 V after injection of 0.5 mM H_2O_2. As shown in Fig. 8A, the response of the modified electrode increased sharply with increasing the HQ concentration to the maximal value of 0.4 mM, and then tended to steady with further increases in the HQ concentration. Such behavior is typical of a mediator-based sensor [40]. Although a higher concentration of mediator could bring a higher sensitivity, it might produce a larger background current, thus 0.5 mM HQ was chosen in subsequent experiments.

The effect of solution pH on the electrocatalytic reduction of H_2O_2 was investigated in the pH range of 5.0–9.0 by steady-state amperometry at −0.15 V. Fig. 8B shows that the current responses were pH-dependent in 0.5 mM H_2O_2 solution containing 0.5 mM HQ. The reduction current reached its maximum at pH 7.0. This indicated that the Au/SPAN-CS matrix did not alter the optimum pH for redox activity of the immobilized HRP.

Fig. 8C shows the effect of the working potential on the steady-state current of the biosensor in the potential range from −0.05 to −0.25 V in pH 7.0 PBS containing 0.5 mM HQ in the presence of 0.5 mM H_2O_2. The steady-state current increased sharply when the working potential shifted from −0.05 to −0.15 V and then increased slowly for potentials beyond −0.15 V. At −0.15 V, sufficient current response was obtained, the background current was minimized and interference from other electroactive species could be avoided.

With an increasing temperature from 10 to 70 °C, the activity of the immobilized enzymes increased, leading to an increasing amperometric response (Fig. 8D). When the temperature was higher than 40 °C, the amperometric response decreased. The immobilized enzymes showed activity even at 70 °C. It was evident that the immobilized enzymes had a good thermal stability because of the unchangeability of its microenvironment and native structure upon temperature change. For practical convenience, all experiments were carried out at room temperature, at which the response was 94% of that at 40 °C.

3.5. Electrochemical performance of the H_2O_2 biosensor

In 0.1 M pH 7.0 PBS containing 0.5 mM HQ, the CV peak currents of the Au/SPAN-HRP-CS/GCE increased linearly with the square root of scan rate in the range of 25–500 mV/s, as shown in Fig. 9. From the results, we can confirm that a diffusion-controlled process occurred at the Au/SPAN-HRP-CS/GCE, and the proposed reaction mechanism of the biosensor can be summarized as follows [41]:

$$HRP_{(red)} + H_2O_2 \rightarrow HRP_{(ox)} + H_2O \quad (1)$$

$$HRP_{(ox)} + HQ_{(red)} \rightarrow HRP_{(red)} + HQ_{(ox)} \quad (2)$$

$$HQ_{(ox)} + 2H^+ + 2e \rightarrow HQ_{(red)}. \quad (3)$$

First, H_2O_2 in the solution is reduced by the immobilized $HRP_{(red)}$. Then the HRP can be regenerated with the aid of the electron mediator, while the mediator $HQ_{(red)}$ can be oxidized to $HQ_{(ox)}$ in the enzymatic reaction. Finally, the $HQ_{(ox)}$ produced is electrochemically reduce on the electrode and recycles, leading to a great increase of the reduction current, which is indicative of the presence of H_2O_2.

In order to provide further insight into the nature of the increased electrochemical and enzymatic response of the Au/SPAN-HRP-CS/GCE, the current–time response of H_2O_2 at bare GCE (a), SPAN-

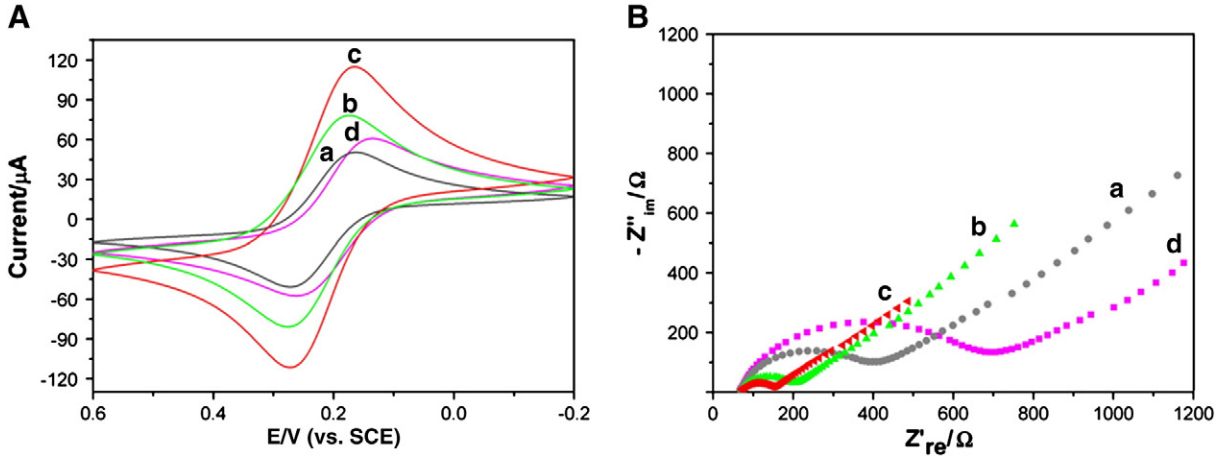

Fig. 7. (A) CVs and (B) Nyquist diagrams recorded at bare GCE (a), SPAN-CS/GCE (b), Au/SPAN-CS/GCE (c) and Au/SPAN-HRP-CS/GCE (d) in pH 7.0 PBS solution containing 0.1 M KCl and 2 mM $Fe(CN)_6^{3-}$/ $Fe(CN)_6^{4-}$.

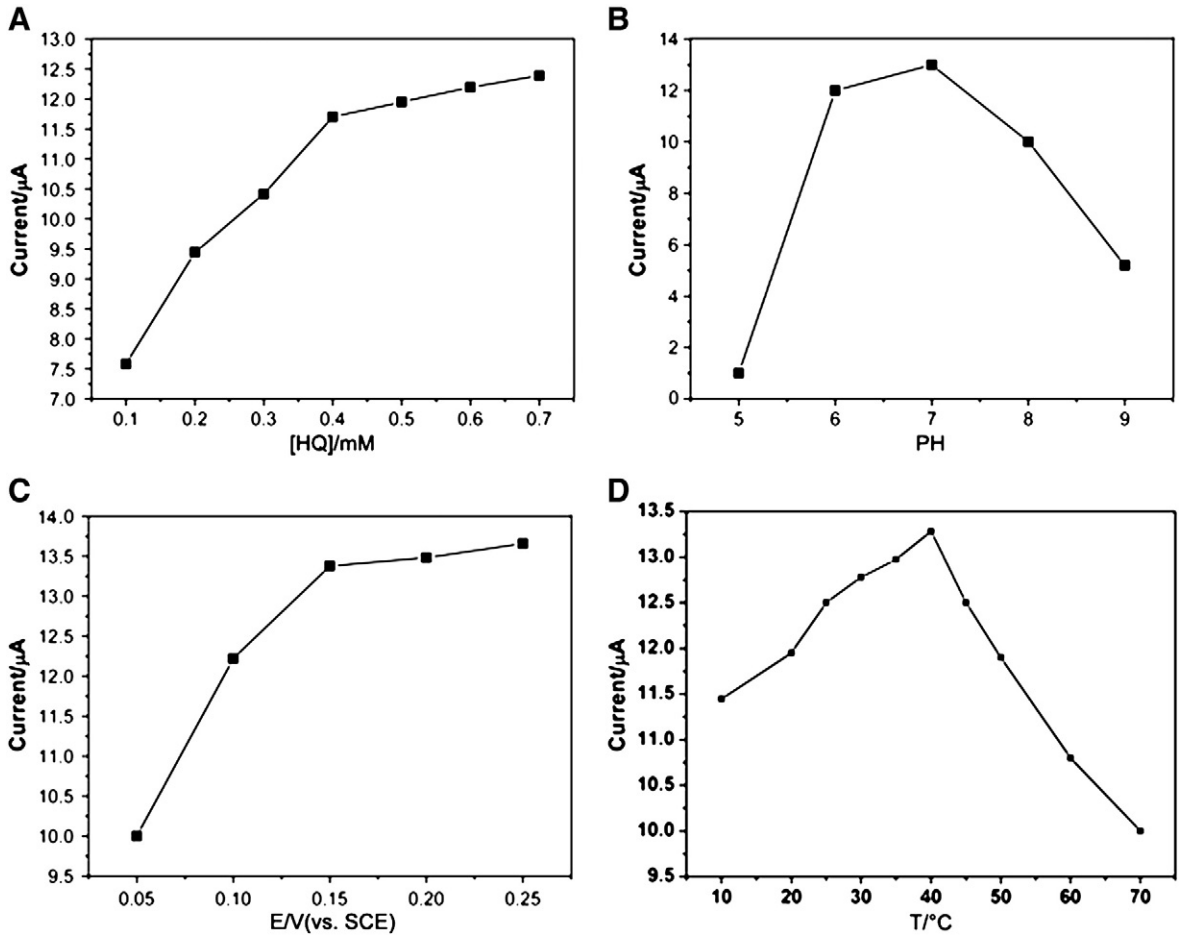

Fig. 8. Dependence of amperometric response of 0.5 mM H_2O_2 at Au/SPAN-HRP-CS/GCE on the (A) concentration of HQ, (B) solution pH, (C) working potential, (D) temperature.

CS/GCE (b), Au/SPAN-CS/GCE (c) and Au/SPAN-HRP-CS/GCE (d) were monitored at −0.15 V during the successive additions of 100 μM H_2O_2 in stirred PBS, as shown in Fig. 10A. The bare GCE had no evident amperometric response when aliquots of H_2O_2 were added. Although SPAN and Au nanoparticles could also catalyze H_2O_2 reduction, the response signals were relatively slender. The Au/SPAN-HRP-CS/GCE exhibited a larger stepped growth of reduction currents and faster response time ($t_{95\%}$<5 s), exhibiting its higher sensitivity. The faster response time and higher sensitivity of Au/SPAN-HRP-CS/GCE might be attributed to the larger electroactive surface area of SPAN and the better ability to facilitate the electron transfer of Au nanoparticles.

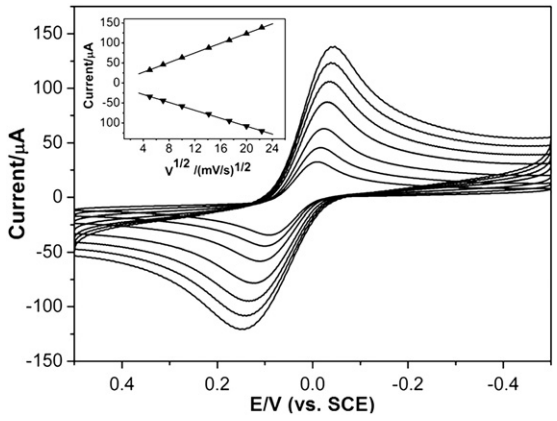

Fig. 9. Cyclic voltammograms of the Au/SPAN-HRP-CS/GCE at 25, 50, 100, 200, 300, 400, 500 mV/s (from internal to external) in 0.1 M pH 7.0 PBS containing 0.5 mM HQ. The inset shows the plots of the peak current vs. $v^{1/2}$.

The typical current–time response for H_2O_2 detection was shown in Fig. 10B. Upon successive addition of H_2O_2 to PBS under optimized conditions, the amperometric response of the sensor increased simultaneously. With the increasing H_2O_2 concentration, the amperometric response increased linearly in the range from 10 to 2000 μM with a correlation coefficient of 0.9998 (n = 30). The regression equation was expressed as $I/\mu A = (0.1151 +/- 0.008) + (20.27 +/- 0.20)\ [H_2O_2]/mM$, with the slope of (20.27 +/− 0.20) μA mM^{-1}. The detection limit of this biosensor was estimated as 1.6 μM at a signal-to-noise ratio of 3. According to the linear equation, we could detect H_2O_2 concentration quantitatively. Higher H_2O_2 levels could be detected by an appropriate dilution with pH 7.0 PBS.

The Au/SPAN-HRP-CS/GCE showed a typical Michaelis–Menten kinetics [42], and the apparent Michaelis–Menten constant (K_m) could be obtained from the electrochemical version of the Lineweaver–Burk equation: $1/I_{ss} = 1/I_{max} + K_m/I_{max}(1/C)$, where I_{ss} is the steady-state current after addition of the substrate, C is the bulk concentration of the substrate, and I_{max} is the maximum current measured under saturated conditions. K_m can be obtained by analysis of the slope and intercept of the plot of the reciprocals of the steady-state current versus H_2O_2 concentration. The K_m value of this H_2O_2 biosensor was determined by steady-state amperometric response to be approximately 2.21 mM, which was smaller than that of the previous reports [43,44]. The smaller K_m value means that the immobilized HRP has higher enzymatic activity, and that the biosensor has greater affinity and catalytic performance towards H_2O_2. The performance (in terms of linear detection range, detection limit and K_m) of the Au/SPAN-HRP-

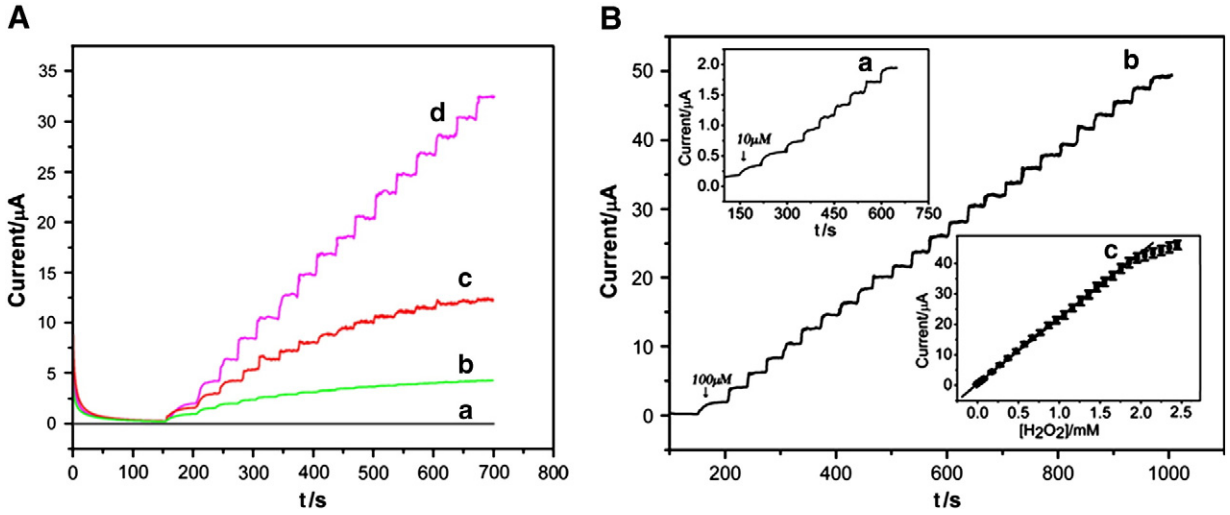

Fig. 10. (A) Amperometric response of successive addition of 100 μM H_2O_2 at bare GCE (a), SPAN-CS/GCE (b), Au/SPAN-CS/GCE (c) and Au/SPAN-HRP-CS/GCE (d) in 0.1 M PBS (pH 7.0) containing 1 mM HQ. The applied potential is −0.15 V. (B) Amperometric response of Au/SPAN-HRP-CS/GCE to the successive addition of 10 μM H_2O_2 (a) or 100 μM H_2O_2 (b) at the applied potential of −0.15 V in 0.1 M PBS (pH 7.0) containing 1 mM HQ; (c) calibration curve.

CS/GCE as a H_2O_2 biosensor is compared with earlier reported H_2O_2 biosensors and is presented in Table 1.

3.6. Reproducibility and stability of the developed H_2O_2 biosensor

The reproducibility and stability are the two important parameters for the evaluation of biosensor to be applied for analytical purposes. The detection reproducibility of Au/SPAN-HRP-CS/GCE in the online assay for 200 μM H_2O_2 was measured. High reproducibility of the amperometric response (R.S.D. of 3.2%) was observed for 10 repetitive injections of 200 μM H_2O_2 in PBS. The stability of the Au/SPAN-HRP-CS/GCE was performed by measuring the current response of the biosensor in pH7.0 PBS with 200 μM H_2O_2. The response of Au/SPAN-HRP-CS/GCE can retain 95% of its original signal after 15 days storage. For comparison, the stability of Au/SPAN-HRP/GCE and the processed biosensor without GA were also explored under the same situation; they kept 80% and 60% of their initial response current after 10 days, suggesting that CS and GA are contributive to the stability of the immobilized Au/SPAN-HRP biocomposite. The better stability of Au/SPAN-HRP-CS/GCE may also be attributed to the excellent biocompatibility of Au nanoparticles coated SPAN nanofibers that offered a favorable microenvironment to the immobilized HRP. After 1 month storage, the bio-electrode retained about 85% of its original current response.

3.7. Selectivity of the developed H_2O_2 biosensor

Discrimination of interfering species having electro-activities similar to the target analyte is one of the most important analytical aspects for an amperometric biosensor. Ascorbic acid (AA) and uric acid (UA) are the most common interfering electroactive species during the amperometric detection of H_2O_2. The interference determination was investigated by comparing the responses between before and after adding of AA and UA, respectively and together. The changes of the response current could be neglected. This result revealed that the tested interferon could not cause any observable interference for the determination of H_2O_2 at a potential of −0.15 V, indicating high selectivity.

Table 1
Comparison of the analytical performance of different H_2O_2 biosensors.

Different H_2O_2 biosensors	Linear range	Detection limit/μM	K_m/mM	Reference
HRP-ZrO_2/Au	0.02–9.45 mM	2	8.01	[43]
HRP-PANI-EMIES/FTO	1–20 mM	–	27.11	[44]
Au-ME-CoTCAPc/Au	0.5–5 μM	0.2	–	[45]
silica/HRP–HAp/GCE	1–100 μM	0.35	0.0218	[46]
Ti/TiO_2/Au/HRP/GCE	5–400 μM	2	–	[47]
HRP/nanogold/PTH/nanogold/CPE	9.6–1200 μM	0.75	0.25	[48]
Au-SPAN/HRP/GCE	10–2000 μM	1.6	2.21	Present work

3.8. H_2O_2 determination in real sample

To further assess the possible application of our proposed sensor for real sample analysis, the concentration of H_2O_2 in commercial contact lens care solution was determined. The real sample was diluted to different concentrations (100 to 1000 μM) with pH7.0 PBS buffer. The mean concentration of H_2O_2 in the sample for five successive assays was determined to be 0.973 M by using the proposed sensor (RSD = 3.5%), which was close to the value of 0.992 M by the traditional potassium permanganate titration.

4. Conclusions

Au/SPAN nanofibers with grooves have been prepared and TEM, SEM, IR, TG and electrochemical techniques have been used to characterize the nanocomposites. The doping of oxygen-containing groups on SPAN could maintain its good electro-activity in medium with higher pH values, and the modification of Au nanoparticles might provide a biocompatible microenvironment for the immobilization of enzyme. The resulting Au/SPAN-HRP-CS/GCE has been used as a sensor for detecting the electrocatalytic reduction of H_2O_2 in the presence of HQ as mediator, with a low detection limit and rapid response time. Furthermore, the biosensor possessed satisfactory stability, reproducibility and selectivity. So the Au/SPAN could not only be suitable for the immobilization of HRP, but also have potential applications in the fabrication of other enzyme-based biosensor.

Acknowledgements

We greatly appreciate the support from the National Natural Science Foundation of China (20905035, 20805030), Youth Scientific Development Foundation of NJUT (39704002) and MOE Key Laboratory of Analytical Chemistry for Life Science (KLACLS1012). This work

is also sponsored by Qing Lan Project of Education Department of Jiangsu Province.

References

[1] M. Bruchez, M. Moronne, P. Gin, S. Weiss, A.P. Alivisatos, Semiconductor nanocrystals as fluorescent biological labels, Science 281 (1998) 2013–2016.
[2] X. Gan, T. Liu, J. Zhong, X.J. Liu, G.X. Li, Effect of silver nanoparticles on the electron transfer reactivity and the catalytic activity of myoglobin, ChemBioChem 5 (2004) 1686–1691.
[3] Z.H. Wen, S.Q. Ci, J.H. Li, Pt nanoparticles inserting in carbon nanotube arrays: nanocomposites for glucose biosensors, J. Phys. Chem. C 113 (2009) 13482–13487.
[4] C.P. Reis, R.J. Nenfeld, A.J. Ribeiro, F. Veiga, Nanoencapsulation II. Biomedical applications and current status of peptide and protein nanoparticulate delivery systems, Nanomedicine 2 (2006) 53–65.
[5] Y.N. Xia, P.D. Yang, Y.G. Sun, Y.Y. Wu, B. Mayers, B. Gates, Y.D. Yin, F. Kim, H.Q. Yan, One-dimensional nanostructures: synthesis, characterization, and applications, Adv. Mater. 15 (2003) 353–389.
[6] L.M. Li, J. Huang, T.H. Wang, H. Zhang, Y. Liu, J.H. Li, An excellent enzyme biosensor based on Sb-doped SnO_2 nanowires, Biosens. Bioelectron. 25 (2010) 2436–2441.
[7] M. Ahmad, C.F. Pan, Z.X. Luo, J. Zhu, A Single ZnO nanofiber-based highly sensitive amperometric glucose biosensor, J. Phys. Chem. C 114 (2010) 9308–9313.
[8] T.J. Zhang, W. Wang, D.Y. Zhang, X.X. Zhang, Y.R. Ma, Y.L. Zhou, L.M. Qi, Biotemplated synthesis of gold nanoparticle–bacteria cellulose nanofiber nanocomposites and their application in biosensing, Adv. Funct. Mater. 20 (2010) 1152–1160.
[9] Q.L. Sheng, J.B. Zheng, X.D. Shang-Guan, W.H. Lin, Y.Y. Li, R.X. Liu, Direct electrochemistry and electrocatalysis of heme-proteins immobilized in porous carbon nanofiber/room-temperature ionic liquid composite film, Electrochim. Acta 55 (2010) 3185–3191.
[10] X.H. Kang, J. Wang, H. Wu, I.A. Aksay, J. Liu, Y.H. Lin, Glucose oxidase–graphene–chitosan modified electrode for direct electrochemistry and glucose sensing, Biosens. Bioelectron. 25 (2009) 901–905.
[11] S. Yang, W.Z. Jia, Q.Y. Qian, Y.G. Zhou, X.H. Xia, Simple approach for efficient encapsulation of enzyme in silica matrix with retained bioactivity, Anal. Chem. 81 (2009) 3478–3484.
[12] J. Li, X.Q. Lin, Glucose biosensor based on immobilization of glucose oxidase in poly (o-aminophenol) film on polypyrrole-Pt nanocomposite modified glassy carbon electrode, Biosens. Bioelectron. 22 (2007) 2898–2905.
[13] D. Ivnitski, K. Artyushkova, R.A. Rincn, P. Atanassov, H.R. Luckarift, G.R. Johnson, Entrapment of enzymes and carbon nanotubes in biologically synthesized silica: glucose oxidase-catalyzed direct electron transfer, Small 4 (2008) 357–364.
[14] V. Vamvakaki, M. Hatzimarinaki, N. Chaniotakis, Biomimetically synthesized silica–carbon nanofiber architectures for the development of highly stable electrochemical biosensor systems, Anal. Chem. 80 (2008) 5970–5975.
[15] S. Wolfgang, Electron-transfer pathways in amperometric biosensors. Ferrocene-modified enzymes entrapped in conducting-polymer layers, Biosens. Bioelectron. 10 (1995) 181–193.
[16] R. Arunas, H. Katja, C. Elisabeth, L. Valdas, S. Wolfgang, Polypyrrole-entrapped quinohemoprotein alcohol dehydrogenase. Evidence for direct electron transfer via conducting-polymer chains, Anal. Chem. 71 (1999) 3581–3588.
[17] U. Lange, N.V. Roznyatovskaya, V.M. Mirsky, Conducting polymers in chemical sensors and arrays, Anal. Chim. Acta 614 (2008) 1–26.
[18] C.A.K. Wei, Md.A. Rahman, E.S. Choe, K.L. Dong, Y.B. Shim, A novel biosensor based on activation effect of thiamine on the activity of pyruvate oxidase, Biosens. Bioelectron. 23 (2008) 1374–1381.
[19] N. Oyama, T. Tatsuma, T. Sato, T. Sotomura, A kinase-cyclin pair in the RNA polymerase II holoenzyme, Nature 373 (1995) 598–600.
[20] S. Mu, J. Ye, Y. Wang, A rechargeable $Zn/ZnCl_2$, NH_4Cl/polyaniline/carbon dry battery, J. Power Sources 45 (1993) 153–159.
[21] M. Kanungo, A. Kumar, A.Q. Contractor, Microtubule sensors and sensor array based on p olyaniline synthesized in the presence of poly(styrene sulfonate), Anal. Chem. 75 (2003) 5673–5679.
[22] A.J. Killard, S. Zhang, H. Zhao, R. John, E.I. Iwuoha, M.R. Smyth, Development of an electrochemical flow injection immunoassay (FIIA) for the real-time monitoring of biospecific interactions, Anal. Chim. Acta 400 (1999) 109–119.
[23] Y.C. Luo, J.S. Do, Urea biosensor based on PANi(urease)-Nafion/Au composite electrode, Biosens. Bioelectron. 20 (2004) 15–23.
[24] L. Shi, Y. Xiao, I. Willner, Electrical contacting of glucose oxidase by DNA-templated polyaniline wires on surfaces, Electrochem. Commun. 6 (2004) 1057–1060.
[25] Q. Lu, C.M. Li, One-step co-electropolymerized conducting polymer–protein composite film for direct electrochemistry-based biosensors, Biosens. Bioelectron. 24 (2008) 767–772.
[26] L. Zhang, C.H. Zhang, J.Y. Lian, Electrochemical synthesis of polyaniline nanonetworks on p-aminobenzene sulfonic acid functionalized glassy carbon electrode: its use for the simultaneous determination of ascorbic acid and uric acid, Biosens. Bioelectron. 24 (2008) 690–695.
[27] J. Yue, A.J. Epstein, Synthesis of self-doped conducting polyaniline, J. Am. Chem. Soc. 112 (1990) 2800–2801.
[28] L. Zhang, J.Y. Lian, Growth of biofilms on an electrode surface and its application in electrochemical biosensoring, J. Electroanal. Chem. 611 (2007) 51–59.
[29] L. Zhang, Z.G. Shi, Q.H. Lang, J. Pan, Electrochemical synthesis of belt-like polyaniline network on p-phenylenediamine functionalized glassy carbon electrode and its use for the direct electrochemistry of horse heart cytochrome c, Electrochim. Acta 55 (2010) 641–647.
[30] Z. Wang, L. Jiao, T. You, L. Niu, S. Dong, A. Ivaska, Electrochemical preparation of self-doped poly (o-aminobenzenesulfonic acid-co-aniline) microflowers, Electrochem. Commun. 7 (2005) 875–878.
[31] W. Zhang, T. Yang, X. Li, D.B. Wang, K. Jiao, Conductive architecture of Fe_2O_3 microspheres/self-doped polyaniline nanofibers on carbon ionic liquid electrode for impedance sensing of DNA hybridization, Biosens. Bioelectron. 25 (2009) 428–434.
[32] C.X. Lei, S.Q. Hu, G.L. Shen, R.Q. Yu, Immobilization of horseradish peroxidase to a nano-Au monolayer modified chitosan-entrapped carbon paste electrode for the detection of hydrogen peroxide, Talanta 59 (2003) 981–988.
[33] F. Vianello, L. Zennaro, A. Rigo, A coulometric biosensor to determine hydrogen peroxide using a monomolecular layer of horseradish peroxidase immobilized on a glass surface, Biosens. Bioelectron. 22 (2007) 2694–2699.
[34] C.Q. Zhang, G. Li, H.R. Peng, Large-scale synthesis of self-doped polyaniline nanofibers, Mater. Lett. 63 (2009) 592–594.
[35] W. Yan, X.M. Feng, X.J. Chen, W.H. Hou, J.J. Zhu, A super highly sensitive glucose biosensor based on Au nanoparticles–AgCl@polyaniline hybrid material, Biosens. Bioelectron. 23 (2008) 925–931.
[36] Z. Wei, L. Zhang, M. Yu, Y. Yang, M. Wan, Self-assembling sub-micrometer-sized tube junctions and dendrites of conducting polymers, Adv. Mater. 15 (2003) 1382–1385.
[37] G. Li, Z. Zhang, Synthesis of dendritic polyaniline nanofibers in a surfactant gel, Macromolecules 37 (2004) 2683–2685.
[38] S. Quilard, G. Louran, J.P. Buisson, S. Lefra, J. Marters, A.G. MacDiarmid, Vibrational analysis of the reduced form of polyaniline: the leucoemeraldine base, Synth. Met. 50 (1992) 525–530.
[39] Y. Wei, K.F. Hsueh, Thermal analysis of chemically synthesized polyaniline and effects of thermal aging on conductivity, J. Polym. Sci., Part A: Polym. Chem. 27 (1989) 4351–4363.
[40] Y. Xiao, H.X. Ju, H.Y. Chen, Hydrogen peroxide sensor based on horseradish peroxidase-labeled Au colloids immobilized on gold electrode surface by cysteamine monolayer, Anal. Chim. Acta 391 (1999) 73–82.
[41] S.H. Chen, R. Yuan, Y.Q. Chai, L. Xu, N. Wang, X.N. Li, L.Y. Zhang, Amperometric hydrogen peroxide biosensor based on the immobilization of horseradish peroxidase (HRP) on the layer-by-layer assembly films of gold colloidal nanoparticles and toluidine blue, Electroanalysis 18 (2006) 471–477.
[42] R.A. Kamin, G.S. Wilson, Rotating ring-disk enzyme electrode for biocatalysis kinetic studies and characterization of the immobilized enzyme layer, Anal. Chem. 52 (1980) 1198–1205.
[43] Z.Q. Tong, R. Yuan, Y.Q. Chai, Y. Xie, S.H. Chen, A novel and simple biomolecules immobilization method: electro-deposition ZrO_2 doped with HRP for fabrication of hydrogen peroxide biosensor, J. Biotechnol. 128 (2007) 567–575.
[44] P.N. Mashazi, K.I. Ozoemena, T. Nyokong, Tetracarboxylic acid cobalt phthalocyanine SAM on gold: potential applications as amperometric sensor for H_2O_2 and fabrication of glucose biosensor, Electrochim. Acta 52 (2006) 177–186.
[45] P. Wang, S.Q. Li, J.Q. Kan, A hydrogen peroxide biosensor based on polyaniline/FTO, Sens. Actuat. B 137 (2009) 662–668.
[46] B. Wang, J.J. Zhang, Z.Y. Pan, X.Q. Tao, H.S. Wang, A novel hydrogen peroxide sensor based on the direct electron transfer of horseradish peroxidase immobilized on silica–hydroxyapatite hybrid film, Biosens. Bioelectron. 24 (2009) 1141–1145.
[47] A.K.M. Kafi, G.S. Wu, A.C. Chen, A novel hydrogen peroxide biosensor based on the immobilization of horseradish peroxidase onto Au-modified titanium dioxide nanotube arrays, Biosens. Bioelectron. 24 (2008) 566–571.
[48] F.C. Wang, R. Yuan, Y.Q. Chai, A new amperometric biosensor for hydrogen peroxide determination based on HRP–nanogold–PTH–nanogold-modified carbon paste electrodes, Eur. Food Res. Technol. 225 (2007) 95–104.